LA-9838-MS

C.3

Neutron Production by Alpha Particles in Thin Uranium Hexafluoride

Los Alamos
Los Alamos National Laboratory
Los Alamos, New Mexico 87545

Edited by Sarah Kreiner, Group Q-1
Prepared by Sophia Howard, Group Q-1

Neutron Production by Alpha Particles in Thin Uranium Hexafluoride

J. E. Stewart

CONTENTS

NEUTRON PRODUCTION BY ALPHA PARTICLES IN THIN URANIUM HEXAFLUORIDE

by

J. E. Stewart

ABSTRACT

Alpha-particle-induced neutrons from UF_6 serve as an indicator of ^{235}U enrichment and may be exploited for safeguards purposes. If the UF_6 density is low enough, neutron production is reduced as a result of alpha-particle escape before (α,n) reactions with ^{19}F. Calculational methods and results are presented that enable prediction of neutron production in low-density ("thin") UF_6 as encountered in the gas centrifugation method of uranium enrichment. Neutron production is shown to be strongly dependent on average UF_6 density and weakly dependent on rotational speed in an operating centrifuge.

I. INTRODUCTION

Neutron production by uranium (predominantly ^{234}U) decay alpha particles reacting with ^{19}F atoms in UF_6 is correlated with $^{235}UF_6$ enrichment. As the fraction of $^{235}UF_6$ is increased by the centrifuge enrichment process, the $^{234}UF_6$ fraction is increased even more. The elevated neutron production from $^{234}UF_6$ allows detection of highly enriched uranium (HEU) by neutron detectors monitoring cascades of operating gas centrifuges.[1-4]

Energies of the primary ^{234}U decay alpha particles are 4.721 (28%) and 4.773 (72%) MeV (Ref. 5). The threshold energy for the (α,n) reaction in ^{19}F is 2.36 MeV (Ref. 6). A "thick target" for neutron production in UF_6 exists if the target depth (product of the UF_6 atom density and the characteristic dimension of the UF_6 volume in question) is sufficient to allow a ^{234}U decay alpha particle to slow to an energy below the (α,n) threshold value while still in the UF_6 volume. A comparison of measured[7] and calculated UF_6 thick-target neutron yields is given in Ref. 5.

A thick-target neutron production model is not directly applicable to low-density UF_6 gas, where alpha particles may escape the gas volume at energies above the $^{19}F(\alpha,n)$ cross-section threshold. Such "thin-target" situations are encountered in the gas centrifugation process for UF_6 enrichment. A method used for thick-target neutron production calculations was modified and used to compute the probability of neutron production by an alpha particle of initial energy E_0 before escape at final energy E_f (Ref. 8). For a given initial energy E_0, the escape energy E_f can be directly related to the total path length $L(E_0 \rightarrow E_f)$ and projected range $R(E_0 \rightarrow E_f)$ traversed by the particle from birth to escape. Hence, by using a Monte Carlo code for ray tracing, the effective alpha-induced neutron production from the distribution of UF_6 gas in an operating centrifuge may be computed.

II. THIN-TARGET NEUTRON PRODUCTION THEORY

The probability that an alpha particle of initial energy E_0 will produce a neutron by an (α,n) reaction within a material with macroscopic (α,n) cross-section $\Sigma(E)$ and stopping power $dE/dx(E)$ before escaping at energy E_f is given by

$$P(E_0 \rightarrow E_f) = \int_{E_0}^{E_f} \frac{\Sigma(E)}{dE/dx(E)} \, dE \quad \left(\frac{\text{neutrons}}{\alpha}\right) \quad . \tag{1}$$

Note that setting E_f to zero in Eq. (1) yields the thick-target neutron production value. A plot showing computed values of $P(E_0 \rightarrow E_f)$ for the three initial alpha-particle energies of ^{234}U is given in Ref. 8 and reproduced here as Fig. 1. Figure 1 shows that maximum neutron production is reached after the alpha particle slows to approximately 2.5 MeV. No additional neutrons are produced after the alpha-particle energy falls below the threshold value for ^{19}F (2.36 MeV). The total path length traversed by the alpha particle in slowing from initial energy E_0 to final energy E_f is given by

$$L(E_0 \rightarrow E_f) = N \int_{E_0}^{E_f} \frac{dE}{dE/dx(E)} \quad \left(\frac{\text{atoms}}{\text{cm}^2}\right) \quad , \tag{2}$$

where N is the atomic density of the slowing-down material.

Energetic alpha particles dissipate energy in inelastic collisions that result in ionization and excitation of the surrounding atoms. The alpha-particle trajectory is affected only slightly in small momentum transfers with electrons; that is, the paths of energetic alpha particles tend to be straight.[9,10] Figure 2 displays $L(E_0 \rightarrow E_f)$ vs E_f computed by numerically evaluating the integral in Eq. (2) for an initial alpha-particle energy of 4.773 MeV with UF_6 as the slowing-down material. Along with the total path length, the projected range $R(E_0 \rightarrow E_f)$ is also shown in Fig. 2. As the names imply, projected range refers to the straight-line distance from point-of-origin of the alpha particle and total path length refers to the total distance traveled. As defined here, total path length and projected range have units of length times atomic density. The relationships between total path length and projected range for alpha particles slowing in uranium and fluorine were taken from Ref. 11.

To use the "thin-target" neutron production data efficiently in Monte Carlo ray-tracing calculations, a data set was formed with projected range as
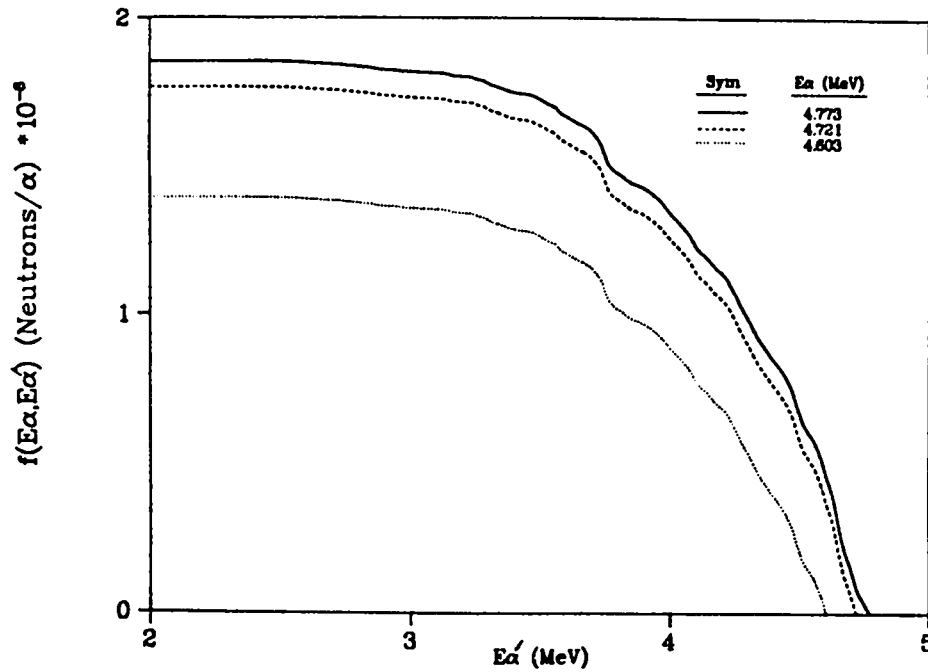
3

Fig. 1. Neutron production probability for the 4.603-, 4.721-, and 4.773-MeV alpha particles of ^{234}U in UF$_6$ before escape at energy E_α'.
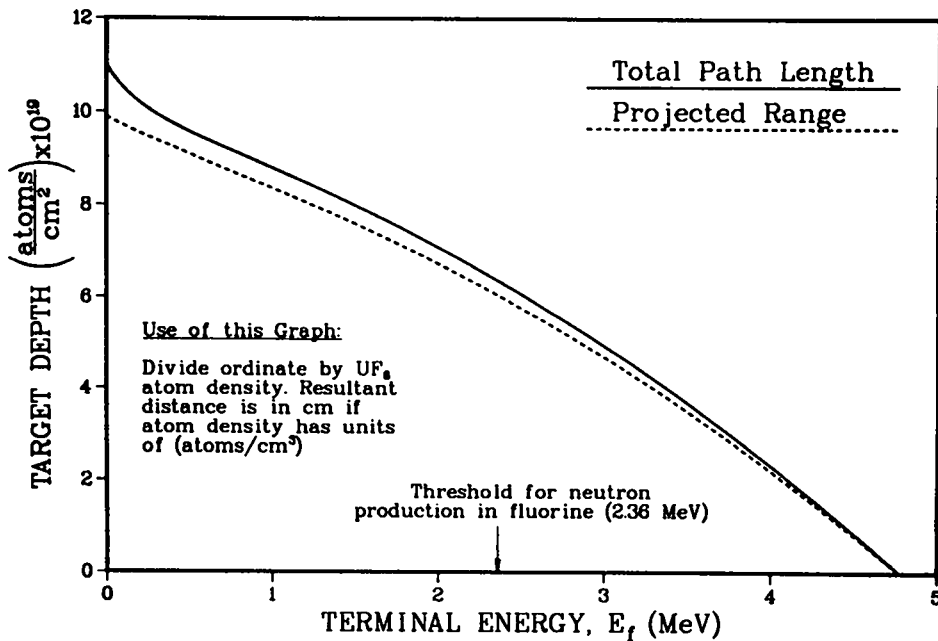

Fig. 2. Total path length and projected range of a 4.773-MeV alpha particle in UF$_6$ vs terminal energy.

the independent variable. These data are plotted in Fig. 3, showing neutron production by a 4.773-MeV alpha particle vs projected range in UF_6. This plot was fitted (with a maximum deviation of 22%) using the formula

$$P(R) = 0.95 + 0.53 \ln R \ . \tag{3}$$

Once neutron production could be associated with projected range, it was possible to apply an existing Monte Carlo code to solve the geometry-dependent part of the problem. That is, the effective average neutron production was determined for geometries of interest by using the code to compute the alpha-particle projected ranges, associating these with neutron production by the use of Eq. (3), and accumulating the appropriate averages.

A calculational model of the distribution of UF_6 density within the spinning rotor of an operating gas centrifuge was constructed for use in the Monte Carlo simulations of the alpha-particle transport process, including neutron
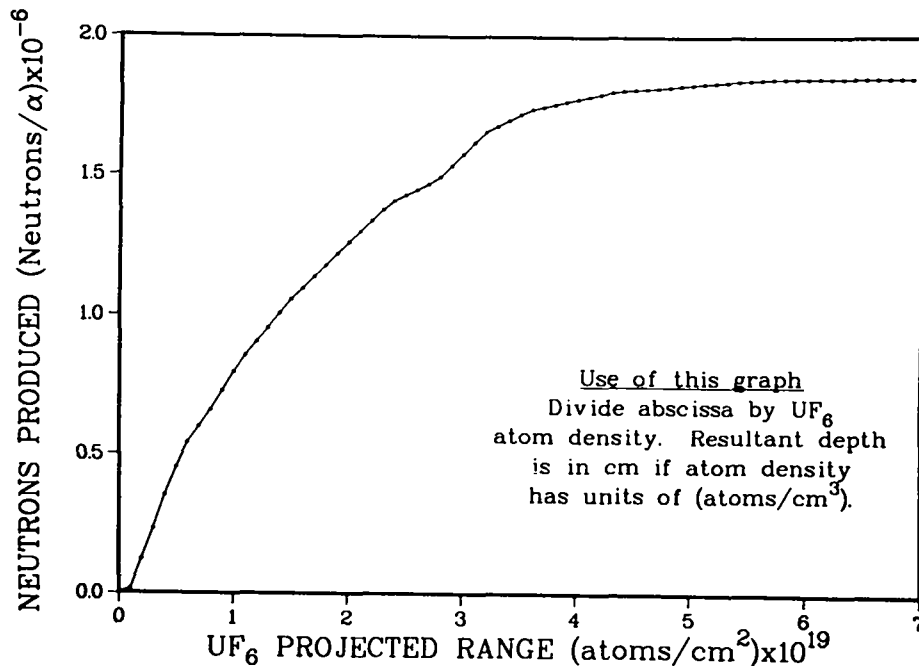
Use of this graph
Divide abscissa by UF_6 atom density. Resultant depth is in cm if atom density has units of $(atoms/cm^3)$.

Fig. 3. Neutron production by a 4.773-MeV alpha particle vs projected range in UF_6.

5

production. Figure 4 shows a schematic of the centrifuge rotor and indicates the operational UF_6 distribution. Integrating the radial component of the momentum equation, using the ideal gas law,[12] and rearranging yields an approximate expression for the radial UF_6 density distribution. The UF_6 mass density ρ at radius r is given as a function of the wall mass density $\rho(a)$ by the expression

$$\rho(r) = \rho(a) \exp[-A^2(1 - r^2/a^2)] \quad , \tag{4}$$

where
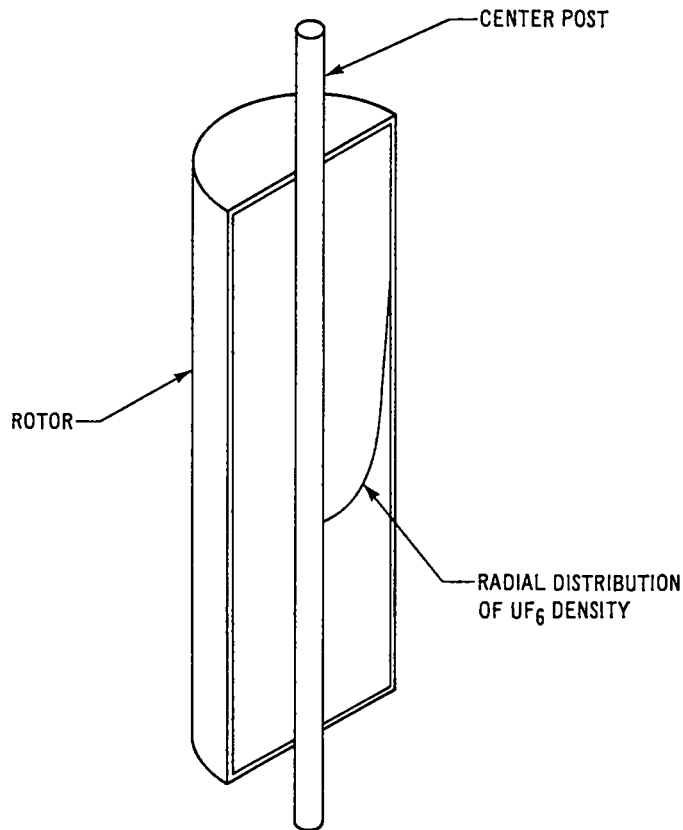
$$A^2 = \frac{M \Omega^2 a^2}{2 R T_0} \quad . \tag{5}$$

Fig. 4. The centrifuge rotor, indicating operational UF_6 distribution.

M is the UF_6 molar mass, Ωa is the rotational velocity of the rotor wall, R is the ideal gas constant, and T_0 is temperature in Eq. (5). The differential mass element for UF_6 gas between the rotor center post ($r = r_0$) and the rotor wall ($r = a$) for a rotor of height h is given by

$$dm = 2\pi h \; \rho(r)rdr \quad . \tag{6}$$

Integrating the mass element between r and a and normalizing yields an expression for the fraction of UF_6 lying between r and a. The fraction F is given by

$$F = \frac{1 - e^{-y}}{1 - e^{-y_0}} \quad , \tag{7}$$

where

$$y = -A^2(1 - r^2/a^2) \quad , \tag{8}$$

and

$$y_0 = -A^2(1 - r_0^2/a^2) \quad . \tag{9}$$

Manipulation of Eq. (7) yields the formula

$$r/a = \left[1 + \frac{\ln(1 - F')}{A^2} \right]^{1/2} \tag{10}$$

7

where

$$F' = F(1 - e^{-y_0}) \ . \tag{11}$$

For Monte Carlo transport simulations, a special source subroutine was prepared for the MCNP code[13] to specify the initial conditions of alpha particles. Equation (10) was used in the source subroutine to sample for the starting position. Particles were transported in a geometry similar to that of Fig. 4. The UF_6 gas volume inside the centrifuge rotor was divided into 10 radial zones. For each case considered, zone boundaries were adjusted so that 10% of the UF_6 gas was contained in each zone. In the transport simulation, straight-line alpha-particle paths were tracked through the zones of varying UF_6 density. As particles crossed zone boundaries, projected range was accumulated. At the point of escape from the geometry, the neutron production associated with the accumulated projected range was recorded using Eq. (3) and a special tally subroutine. Enough particle histories were simulated to satisfy a preset statistical precision.

III. CALCULATIONAL RESULTS AND CONCLUSIONS

The data and methods described above were used to calculate neutron production for a gas centrifuge rotor model representative of United States technology. Neutron production relative to the thick-target value was computed over a range of operating parameters. Figure 5 shows relative thin-target neutron production vs average UF_6 density for a fixed rotor speed. The figure shows relative neutron production to be a fairly strong function of average UF_6 density over a dynamic range of densities typical of centrifuge operating conditions. Figure 6 shows, for fixed average UF_6 density, the relative neutron production vs rotor speed. Over a large dynamic range, Fig. 6 indicates that relative neutron production is only weakly dependent on the speed of the rotor and thus on the internal UF_6 density distribution. This eases computations considerably.

Source term data, such as those shown in Figs. 5 and 6, are essential to predicting effectiveness of neutron monitor arrays for detecting HEU production
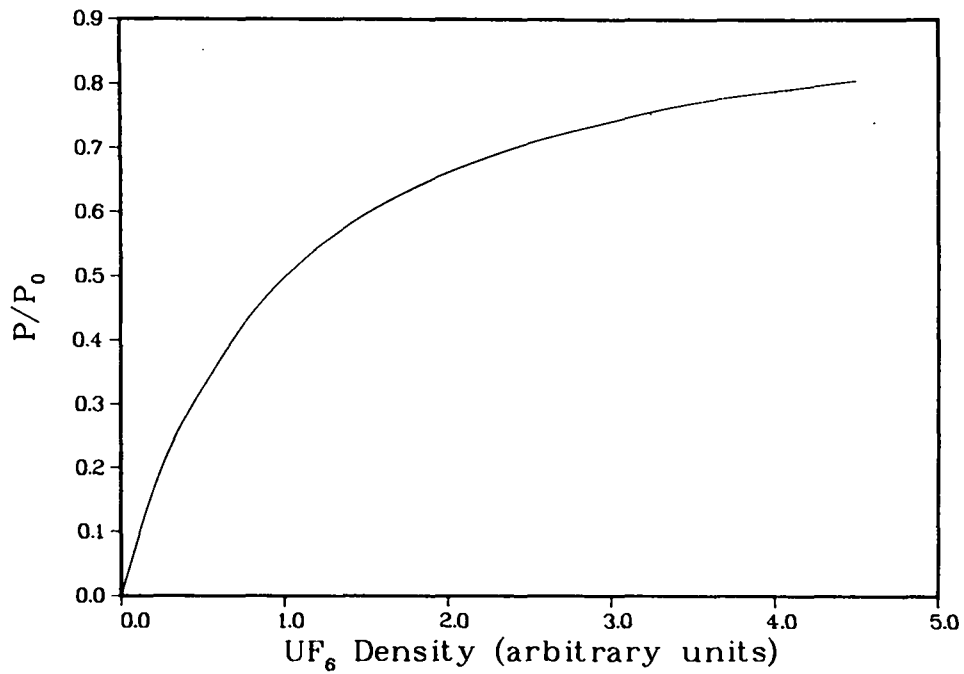
8

Fig. 5. Relative thin-target neutron production in an operating centrifuge vs average UF_6 density.
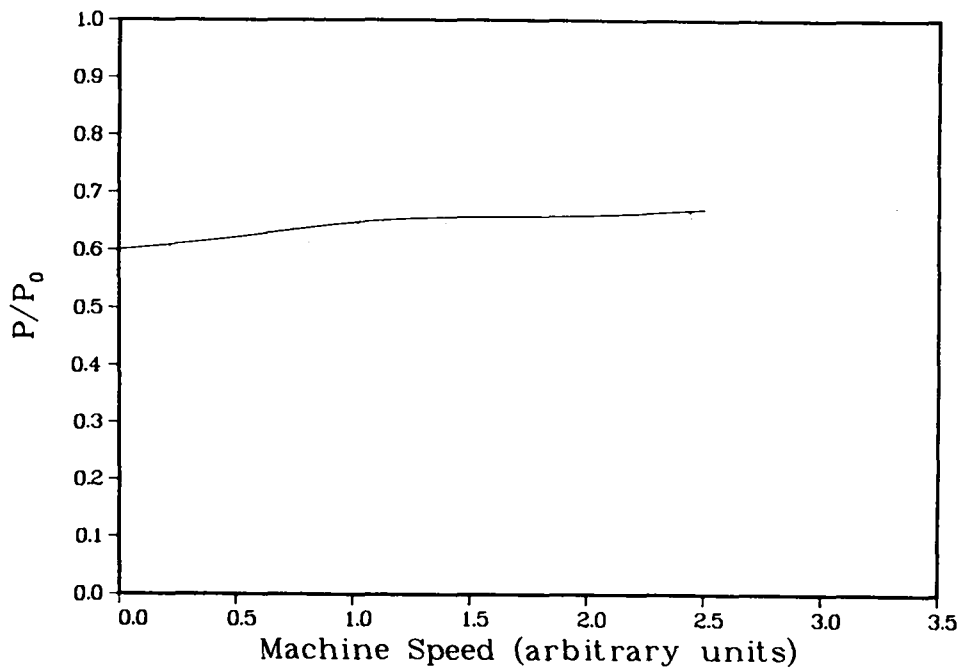

Fig. 6. Relative thin-target neutron production in an operating centrifuge vs machine (rotor) speed.

in centrifuge cascades characteristic of domestic and foreign technology. The calculational methods can be applied in other areas, such as accelerator target design and radiation protection.

ACKNOWLEDGMENTS

REFERENCES

1. R. B. Walton, "Feasibility of Nondestructive Assay Measurements in Uranium Enrichment Plants," Los Alamos Scientific Laboratory report LA-7212-MS (April 1978).

2. J. W. Tape, M. P. Baker, and R. B. Walton, "Conceptual Design of Selected Instrumentation for an International Safeguards System at the Portsmouth Gas Centrifuge Enrichment Plant," in "Nuclear Safeguards Research and Development Program Status Report, January-April 1978," Los Alamos Scientific Laboratory report LA-7439-PR (December 1978).

3. J. E. Stewart, M. Baker, P. Collinsworth, L. Cowder, E. Gallegos, S. Johnson, C. Shonrock, R. Slice, and C. Spirio, "CTF Neutron Monitoring System Design," in "Nuclear Safeguards Research and Development Program Status Report, January-March 1980," Los Alamos Scientific Laboratory report LA-8373-PR (September 1980).

4. J. E. Stewart, J. W. Tape, R. B. Strittmatter, R. Slice, and P. Collinsworth, "Evaluation of CTF Neutron Monitoring System," in "Nuclear Safeguards Research and Development Program Status Report, April-June 1980," Los Alamos National Laboratory Laboratory report LA-8514-PR (February 1981).

5. W. B. Wilson, J. E. Stewart, and R. T. Perry, "Neutron Production in UF_6 from Decay of U Nuclides," Trans. Am. Nucl. Soc. <u>38</u>, 176 (1981).

6. M. Balakrishnan, S. Kailas, and M. K. Mehta, "A Study of the Reaction $^{19}F(\alpha,n)^{22}Na$ in the Bombarding Energy Range 2.6 to 5.1 MeV," Pramana <u>10</u>, 329 (1978).

7. T. E. Sampson, "Neutron Yields from Uranium Isotopes in Uranium Hexafluoride," Nucl. Sci. Eng. $\underline{54}$, 470 (1974).

8. W. B. Wilson, J. E. Stewart, and R. T. Perry, "The $^{19}F(\alpha,n)$ Neutron Production from the Decay of U Nuclides in UF_6," in "Applied Nuclear Data Research and Development, October 1-December 31, 1980," Los Alamos National Laboratory report LA-8757-PR (1981), p. 40.

9. K. Z. Morgan and J. E. Turner, Eds., Principles of Radiation Protection (John Wiley and Sons, Inc., New York, 1967).

10. R. D. Evans, The Atomic Nucleus (McGraw-Hill, New York, 1955).

11. J. F. Ziegler, "Helium Stopping Powers and Ranges in all Elemental Matter," in The Stopping and Ranges of Ions in Matter (Pergamon Press, Inc., New Jersey, 1977), Vol. 4.

12. S. Villani, Ed., Uranium Enrichment, Vol. 35, Topics in Applied Physics (Springer-Verlag, New York, 1979), pp. 184-185.

13. Los Alamos Monte Carlo group, "MCNP - A General Monte Carlo Code for Neutron and Photon Transport, Version 2B," Los Alamos Scientific Laboratory report LA-7396-M, Rev. (November 1979).

Page Range	NTIS Price Code	Page Range	NTIS Price Code	Page Range	NTIS Price Code	Page Range	NTIS Price Code
001-025	A02	151-175	A08	301-325	A14	451-475	A20
026-050	A03	176-200	A09	326-350	A15	476-500	A21
051-075	A04	201-225	A10	351-375	A16	501-525	A22
076-100	A05	226-250	A11	376-400	A17	526-550	A23
101-125	A06	251-275	A12	401-425	A18	551-575	A24
126-150	A07	276-300	A13	426-450	A19	576-600	A25
						601-up*	A99

*Contact NTIS for a price quote.

Los Alamos